Techno-economic assessment of a U-shaped sloshing tank wave energy converter for Italian offshore applications

Renewable Energy 273 (2026) 126067

Contents lists available at ScienceDirect

Renewable Energy

journal homepage: www.elsevier.com/locate/renene

Techno-economic assessment of a U-shaped sloshing tank wave energy converter for Italian offshore applications ☆

Sergej Antonello Sirigu [a,*], Valerio Francesco Barnabei [b], Filippo Giorcelli [a], Giovanni Delibra [b], Alessandro Corsini [b]

[a] Marine Offshore Renewable Energy Lab (MOREnergy Lab), Department of Mechanical and Aerospace Engineering, Politecnico di Torino, Corso Duca degli Abruzzi 24, 10129, Torino, Italy

[b] Department of Mechanical and Aerospace Engineering, Sapienza University of Rome, Rome, Italy

ARTICLE INFO

Keywords:
Wave energy converters
Sloshing tank
Wells turbine
Techno-economic optimisation

ABSTRACT

Wave energy converters (WECs) offer promising opportunities for supplying power to isolated grids and for synergistic co-location with offshore wind farms, particularly in moderate wave climates such as the Mediterranean Sea. This work presents a techno-economic assessment of a floating U-shaped sloshing tank Wave Energy Converter (U-WEC), which exploits the coupled motion of a floating hull and an internal U-tank to drive a Wells turbine-based power take-off. A two-stage optimisation framework is proposed. First, a bi-objective techno-economic optimisation is performed on the main system parameters governing displacement mass, used as a proxy for capital cost, and gross annual energy production. Second, an ad hoc optimisation of the Wells turbine is carried out for each optimal device, accounting for the strong coupling between hull size, resonance behaviour, and turbine operating conditions. The methodology is applied to a Mediterranean site in the Strait of Sicily and compared with a Northern European site to assess the impact of different wave climates. The results show that optimal solutions consistently converge towards asymmetric hull configurations, highlighting the importance of multi-degree-of-freedom hydrodynamic coupling and resonance tuning between the hull and the U-tank. A multi-site assessment across several Italian offshore locations, including offshore wind co-location areas and off-grid islands, confirms the suitability of the proposed U-WEC for Mediterranean offshore applications.

1. Introduction

Over the past decades, growing energy demand and rising CO_2 emissions have driven significant interest in mature renewable technologies like solar, wind, and geothermal power. Ocean waves, an untapped and globally available resource, have also seen numerous proposed harvesting solutions in recent years [1]. However, wave energy remains an emerging technology, and its levelized cost is not yet competitive with other renewables [2]. Among the main factors limiting the maturity of these systems are the wide variety of technological solutions, the harsh marine environment and the challenges in achieving high energy conversion efficiency. In response, many studies have introduced techno-economic optimisation frameworks to pinpoint device geometries and sizes that maximise performance while reducing cost drivers, such as displaced volume, structural mass, and installed power [3]. This technology also benefits from strong complementarity with wind and solar resources, offering excellent opportunities to optimise the energy mix where these resources coexist [4]. In addition, to further lower costs, researchers have investigated synergies between offshore wind and wave farms through shared infrastructure [5]. Recent work has also highlighted that, even in moderate-climate basins such as the Mediterranean, there exist localised wave-energy *hotspots* and island contexts where wave power can contribute meaningfully within hybrid renewable mixes [6].

Most research and proposed solutions have focused on North Sea and European Atlantic coast sites, which feature higher power densities, longer wave periods and significant extreme events. Nonetheless, long-term resource assessments indicate that Mediterranean wave power is expected to remain significant under future climate scenarios [7], thereby motivating site-specific design approaches and accurate resource characterisation, as reported in [8] for Sardinia and in [9] for

☆ This article is part of a Special issue entitled: 'SDEWES2025 - RENE' published in Renewable Energy.

* Corresponding author.
E-mail addresses: sergej.sirigu@polito.it (S.A. Sirigu), valerio.barnabei@uniroma1.it (V.F. Barnabei), filippo.giorcelli@polito.it (F. Giorcelli), giovanni.delibra@uniroma1.it (G. Delibra), alessandro.corsini@uniroma1.it (A. Corsini).

https://doi.org/10.1016/j.renene.2026.126067
Received 19 December 2025; Received in revised form 8 June 2026; Accepted 8 June 2026
Available online 13 June 2026

the Adriatic sea. The Oscillating Water Column (OWC) is among the most extensively studied wave energy converters [10]. In nearshore installations, an OWC captures the rise and fall of water within a chamber to drive bidirectional airflow through a turbine, typically a Wells turbine, which converts it into continuous rotor rotation [11].

Such devices are commonly deployed along coastlines (*e.g.*, the plants of Limpet [12] in Scotland and Pico [13] in the Azores) or integrated into coastal defence structures such as breakwaters [14], combining wave energy harvesting with shoreline protection functions. Beyond coastal infrastructures, several floating OWC concepts have been proposed for offshore deployment, including spar buoy platforms [15] and Backward Bent Duct Buoy devices [16], where the oscillating water column remains in direct communication with the sea. A fundamentally different approach is represented by the UGEN concept, in which wave-induced hull motions drive sloshing within a sealed U-shaped tank, decoupling the internal water column from direct wave action and enabling independent resonance tuning. A related preliminary study by Ribeiro e Silva [17] optimised the hull parameters to maximise the mean power to displacement mass ratio for a Portuguese test site.

Regarding the Wells turbine, research has concentrated on designs tailored to the Mediterranean's characteristic operating regimes [18], on control strategies to boost energy-extraction efficiency [19], and on fluid–structure interaction analyses of flexible turbine blades [20] also for specific applications in WECs systems [21].

Although the Mediterranean Sea has a lower overall wave power density than the North Atlantic and the North Sea, the key issue is not only the reduced resource level, but also the different spectral structure of the local sea states. In particular, Mediterranean offshore locations are generally characterised by shorter dominant wave periods and milder operating conditions than oceanic sites. For WECs, this distinction is crucial because the local wave climate directly affects the system's optimal design parameters. Consequently, pre-designed technologies developed for Atlantic or North Sea conditions are not excluded, but they cannot be assumed to be directly transferable in unchanged form to Italian offshore applications, since devices tuned for longer and more energetic waves may become oversized or off-resonant under Mediterranean conditions. This is precisely why several concepts have been specifically developed for moderate and short-wave climates. In particular, floating offshore inertial devices such as the Pendulum Wave Energy Converter (PeWEC) [22] and the Inertial Sea Wave Energy Converter (ISWEC) [23] have demonstrated favourable performance in short-wave environments. Complementarily, nearshore solutions, including the REsonant Wave Energy Converter (REWEC) [24] and the OBREC overtopping-breakwater concept [25], provide additional examples of technologies tailored to Mediterranean wave climates. Within this framework, the present work investigates a floating U-shaped sloshing tank WEC and develops a techno-economic optimisation procedure for Italian offshore applications. Within this framework, the present work investigates a floating U-shaped sloshing tank WEC, based on the UGEN concept introduced by Ribeiro e Silva [17], extending it through a comprehensive bi-objective techno-economic optimisation framework and a multi-site performance assessment across Italian offshore locations.

1.1. Motivation, novelty and aim of the work

Wave energy technologies are still at an early stage compared with other offshore renewables, and their commercial uptake is hampered by high capital costs, challenging installation and maintenance, and the need for robust yet controllable devices.

Within this context, the present work investigates a floating wave energy converter, named U-WEC that incorporates a U-shaped water sloshing tank within the hull, dynamically coupled with its pitch and surge motions. The resulting oscillatory water flow between the two reservoirs generates a bidirectional airflow that powers Wells turbines installed in the upper ducts. The Power Take Off (PTO) is compact, fully enclosed, and based on the motion of a large internal water mass that can be tuned to resonate with the hull dynamics. These features make the concept particularly suitable for moderate wave climates such as those of the Mediterranean Sea, where compact and site-optimised devices are required.

Previous studies on U-tank WECs have typically focused on limited sets of geometric parameters and on single performance indicators (for example, mean absorbed power or hydrodynamic efficiency), often assuming fixed turbine characteristics and neglecting the techno-economic trade-offs between energy capture and cost drivers. Furthermore, the influence of contrasting metocean conditions on both the optimal hull-U-tank configuration and the associated Wells turbine design has not been analysed in a unified framework.

The present work addresses these gaps by formulating a comprehensive, bi-objective optimisation of a U-shaped sloshing tank WEC. The main novelties can be summarised as follows:

- a fully parametric description of the hull and U-tank, based on ten design variables, combined with a linear frequency-domain model that couples potential-flow hydrodynamics, lumped-parameter sloshing dynamics and an air compression model;
- a techno-economic multi-objective optimisation, where the gross annual energy production AEP_{gross} is maximised while the displacement mass is minimised, the latter acting as a proxy for capital expenditure;
- a dedicated Wells turbine design framework, which generates families of turbine geometries consistent with the device motion and local metocean conditions, and selects the configuration that maximises non-dimensional average power and efficiency;
- a two-site comparison between a Mediterranean location in the Strait of Sicily and a high-energy North Atlantic test site, used to quantify how wave climate reshapes the Pareto frontier and drives systematic trends in hull, U-tank and turbine design;
- performance and efficiency assessments of the novel U-WEC concept at Italian wave-energy hotspots, including three sites of strategic interest for co-location with offshore wind farms and three additional sites relevant for the energy transition of non-interconnected small islands.

This work quantifies the techno-economic performance of the U-WEC at Italian offshore sites and establishes systematic design relationships between wave climate, hull and U-tank resonance tuning, and Wells turbine optimisation.

Overall, the novelty of the present work does not lie in the introduction of a new optimisation paradigm, since techno-economic optimisation approaches are already available in the WEC literature. Rather, it lies in the integrated application of such approaches to a floating U-shaped sloshing-tank WEC, through a unified framework and a site-specific assessment for Mediterranean offshore applications. Instead, from a methodological standpoint, the present two-stage framework is also intended as a first step towards a more advanced co-design paradigm, in which the hydrodynamic system and the Wells turbine will not be treated as separate downstream design tasks, but progressively integrated within a unified optimisation environment.

1.2. Notation

For ease of reference, the notation adopted throughout this work is outlined hereafter. The set of real numbers is denoted by $\mathbb{R}$, while $\mathbb{C}$ indicates the set of complex numbers. For any complex quantity, $\mathrm{Re}(\cdot)$ and $\mathrm{Im}(\cdot)$ denote its real and imaginary parts, respectively, and the imaginary unit is written as j. The symbol 0 is used to represent a zero quantity of appropriate size, irrespective of its dimension. The set of positive integers from 1 to n is written as $\mathbb{N}_n = \{1, 2, \dots, n\}$. Vectors are indicated by bold lowercase letters (e.g. $\boldsymbol{v}$), and matrices by bold uppercase letters (e.g. $\boldsymbol{M}$). Given a matrix $\boldsymbol{M} \in \mathbb{R}^{r\times c}$, its entry in row a and column b is written as $M_{a,b}$, with $a \in \mathbb{N}_r$ and $b \in \mathbb{N}_c$. Similarly, if $\boldsymbol{v} \in \mathbb{R}^s$ is a column vector with s components, its ath element is denoted by v_a, where $a \in \mathbb{N}_s$. The transpose of a matrix or vector is indicated by the superscript ^{T}.

1.3. Structure of the article

The remainder of the article is organised as follows. Section 2 introduces the techno-economic optimisation framework, detailing the chosen objective functions, constraints and constraint-handling strategy, and the adopted algorithm. The same section presents the numerical models used to describe the U-WEC: the frequency-domain hydrodynamic formulation based on potential-flow theory, the lumped-parameter representation of the U-tank sloshing, the air compression model and the resulting state-space assembly of the coupled system. It also describes the geometric parametrisation of the hull and U-tank, and the Wells turbine design framework, including the non-dimensional performance coefficients and the procedure for computing average power and efficiency in irregular seas.

Section 3 outlines the two case-study sites, while Section 4 presents the techno-economic optimisation results. First, the Pareto fronts obtained for the Mediterranean and North Atlantic sites are discussed, highlighting the influence of site conditions on optimal displacement and gross annual energy production AEP_{gross}. Then, the main trends in the optimal design variables are analysed, with emphasis on hull geometry, U-tank tuning and their combined effect on energy capture. The section concludes with a detailed comparison of three representative optimal devices and their associated Wells turbiness, followed by an assessment of their performance at strategically important Italian sites.

Finally, Section 5 summarises the main findings, discusses their implications for the development of U-tank WECs in different wave climates, and outlines directions for future work.

2. Method

Considering the early stage of the WEC technology, the system design optimisation problem is framed as multi-objective, where the two conflicting objective functions are:

- maximisation of the gross annual energy production AEP_{gross}, reflecting hydrodynamic efficiency and control logic performance;
- minimisation of a proxy measure for the total WEC costs, *i.e.* the device displacement mass. Displacement mass was selected as a cost driver because it strongly correlates with capital expenditures, since heavier systems incur higher fabrication, mooring, installation, and transport costs. Given the device's early-stage development, using displacement mass as a proxy for overall project cost provides a clear, representative objective for optimisation [3, 26].

Both objective functions are obtained through numerical simulations of the WEC model, which is described below in the next sections (therefore, no analytical expression of the objective functions is available).

Let $\boldsymbol{d} \in \mathcal{S} \subset \mathbb{R}^{N_d}$ be the design vector whithin the design space $\mathcal{S} \in \mathbb{R}^{N_d}$ containing the continuous and integer parameters fully defining the WEC system under investigation. During the elaboration of the optimisation process, each candidate $\boldsymbol{d}$ is integrated within the numerical model described in the next sections in order to assess the two performance functions defined. Formally, the WEC's design techno-economic optimisation problem reads:

$$\begin{aligned} \min_{\boldsymbol{d}\in\mathcal{S}} \ & [\text{Displacement mass}(\boldsymbol{d}), -AEP_{gross}(\boldsymbol{d})] \\ \text{s.t.} \ & \mathcal{S} = \{\boldsymbol{d} \in \mathbb{R}^{N_d} \mid \boldsymbol{D}_l \le \boldsymbol{d} \le \boldsymbol{D}_u\}, \\ & \boldsymbol{h_d} \le 0, \end{aligned} \tag{1}$$

with $\{\boldsymbol{D}_l, \boldsymbol{D}_u\} \subseteq \mathbb{R}^{N_d}$ the upper and lower bound of the design space $\mathcal{S}$, $\boldsymbol{h_d} \le 0$ the set of constraints concerning geometric, hydrostatic, hydrodynamic and mechanical consistency. In this work, constraint violations are handled by additive death penalties in the fitness functions to steer the search away from unfeasible designs. In particular, for a generic fitness function ($\boldsymbol{f}_{obj}(\boldsymbol{d})$), its value is assessed as:

$$\boldsymbol{f}_{obj}(\boldsymbol{d}) = \begin{cases} \boldsymbol{f}(\boldsymbol{d}) & \text{if feasible device,} \\ \boldsymbol{f}_{death}(\boldsymbol{d}) + \Delta_{death} & \text{if unfeasible device,} \end{cases} \tag{2}$$

where $\boldsymbol{f}_{death}(\boldsymbol{d})$ is a so-called constant death penality function (which has to be opportunely tuned considering the order of magnitude of the function to be optimised) and Δ_{death} is the distance between the unfeasible point and the constraint's violation threshold.

2.1. Working principle and numerical modelling of the U-WEC

In this sub-section we present the working principle and the numerical model used to predict the performance of the U-WEC device and its implementation within the techno-economic optimisation framework. Fig. 1 illustrates the concept of the U-WEC studied here, along with its reference frames. The converter consists of a floating hull, either symmetric or asymmetric in profile, which encloses a U-shaped water tank. The air chamber above the free surface is sealed from the external environment, and the two water columns are connected at the top by one or more ducts accommodating Wells turbines.

Hull motion induced by wave interaction drives water sloshing in the tank, producing bidirectional airflow through the turbines. The Wells turbine, a self-rectifying axial-flow turbine characterised by symmetric blades, produces a unidirectional rotational output even under oscillatory air flow conditions. This enables continuous mechanical power extraction from the alternating airflow without the need for mechanical rectifying systems. The generated mechanical power is subsequently converted into electricity through an electric generator coupled to the turbine shaft.

To ensure efficient computational performance, a frequency-domain modelling approach, commonly adopted in the state of the art, has been employed [27]. Since the device is symmetric about the X-Z plane and extracts energy from the hull's surge and pitch degrees of freedom, waves are preliminarily assumed to be unidirectional and aligned with the hull along the X-axis.[1] Each sea state is modelled as a stationary Gaussian process, and its wave energy spectrum is described through the JONSWAP [29] formulation (as in [30]), parameterised by the significant wave height H_s and peak period T_p.

The hydrodynamic interaction between the incident waves and the hull is represented using linear potential-flow theory [31], which assumes irrotational motion, an incompressible fluid, and a constant mean wetted surface. The frequency-dependent hydrodynamic coefficients (*i.e.* added mass $\boldsymbol{A}(\omega) \in \mathbb{R}^{6\times6}$, radiation damping $\boldsymbol{B}(\omega) \in \mathbb{R}^{4\times4}$, and excitation-diffraction force coefficients $\boldsymbol{F_{exc}}(j\omega) \in \mathbb{C}^6$) are computed through a Boundary Element Method (BEM) [32]. In this work, the open-source solver NEMOH [33] is employed.

Let the hull state vector $\boldsymbol{X} \in \mathbb{R}^6$ be

$$\boldsymbol{X} = [x, y, z, \gamma, \delta, \psi]^T, \tag{3}$$

representing surge, sway, heave, roll, pitch, and yaw, respectively. From established literature [27], the frequency-domain equation of motion of the floater can then be written as

$$[\boldsymbol{M}_{in} + \boldsymbol{A}(\omega)]\ddot{\boldsymbol{X}} + \boldsymbol{B}(\omega)\dot{\boldsymbol{X}} + \boldsymbol{K}_h\boldsymbol{X} = a_w(\omega)\boldsymbol{F}_{exc}(j\omega) + \boldsymbol{F}_{u-tank}, \tag{4}$$

[1] In real offshore conditions, however, directional spreading may redistribute the available wave energy over different incidence angles, modify the excitation of the dominant modes, potentially affecting both the predicted AEP and the optimal design trends. Interest readers can refer to the work of Carapellese et al. [28] for the development of a omni-directional WEC.

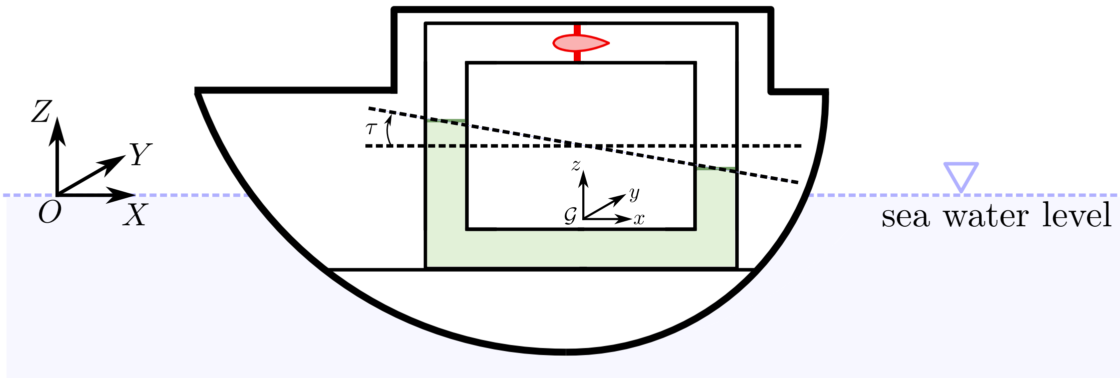

Fig. 1. U-WEC concept sketch and reference systems.

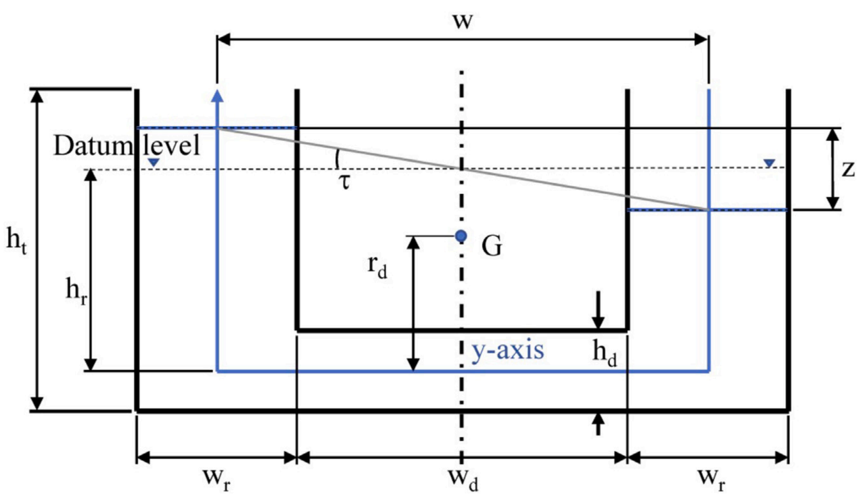

Fig. 2. Reference system and geometrical properties of the U-tank.

where $\boldsymbol{M}_{in} \in \mathbb{R}^{6\times 6}$ is the inertia matrix of the device, $\boldsymbol{K}_h \in \mathbb{R}^{6\times 6}$ is the hydrostatic stiffness matrix, $a_w(\omega)$ is the wave amplitude, and $\boldsymbol{F}_{\boldsymbol{u\text{-}tank}} \in \mathbb{R}^6$ gathers the external forces acting on the hull, including the sloshing-induced inertial forces. The variable ω denotes the wave angular frequency.

Sloshing inside the U-tank is modelled using Lloyd's simplified lumped-parameter analytical model [34], in which the only degree of freedom is the angular displacement τ between the water free-surface levels in the two reservoirs, as sketched in Figs. 1 and 2. Lloyd's model is built on the assumptions of one-dimensional, irrotational flow, small oscillations, and an incompressible fluid, deriving its equations of motion by integrating the one-dimensional Euler equation along the water column.

The result is the following lumped-parameter model, which describes the U-tank sloshing motion as driven by the kinematics imposed by the hull:

$$a_{\tau\tau}\ddot{\tau} + b_{\tau\tau}\dot{\tau} + c_{\tau\tau}\tau = a_{\tau 5}\ddot{x} - a_{\tau 5}\ddot{\delta} - c_{\tau 5}\delta + T_{air}, \tag{5}$$

where T_{air} is the torque acting on the liquid column due to the air compression in the reservoirs. The forces acting on the hull due to the sloshing inside the U-tank can be computed as expressed in Eq. (6):

$$F_{u-tank} = a_{\tau 1}\ddot{\tau} - a_{5\tau}\ddot{\tau} - c_{5\tau}\tau. \tag{6}$$

Within the presented formulation, the constant parameters of the differential equation can be computed from the geometrical properties of the U-tank as:

$$a_{\tau\tau} = Q_t\, w_r \left(\frac{w}{2h_d} + \frac{h_r}{w_r} \right), \tag{7a}$$

$$c_{\tau\tau} = Q_t\, g, \tag{7b}$$

$$b_{\tau\tau} = 2\,\omega_n\, a_{\tau\tau}\, \zeta, \tag{7c}$$

$$a_{\tau 1} = a_{1\tau} = Q_t, \tag{7d}$$

$$a_{\tau 5} = a_{5\tau} = Q_t\,(r_d + h_r), \tag{7e}$$

$$Q_t = \tfrac{1}{2}\,\rho\, w_r\, w^2\, x_t, \tag{7f}$$

where ρ is the water density, x_t the U-tank depth, $\omega_n = \sqrt{c_{\tau\tau}/a_{\tau\tau}}$ the natural frequency of the U-tank, and ζ the damping ratio. The value $\zeta = 0.0087$, adopted in this study, derives from an experimental campaign performed on a small-scale prototype [35].

A duct connects, on the air side, the two reservoirs of the U-tank, and one or more Wells turbines are installed within these ducts to capture the airflow generated by the oscillatory motion of the water column inside the U-tank. To model the airflow inside the U-tank, the water column is treated as a rigid piston that compresses or expands the air in the two reservoirs. Furthermore, the air is assumed to behave as an ideal gas undergoing an isentropic process. In this preliminary assessment, we assume that the Wells turbine behaves as an ideal linear orifice [36], described by Eq. (8):

$$\dot{m} = \alpha \Delta P, \tag{8}$$

where $\dot{m}$ is the air flow mass, ΔP is the air pressure difference between the two reservoirs of the U-tank and α is the linear discharge coefficient. Applying mass conservation and linearising the governing equations, the pressure difference between the two reservoirs is obtained as the state variable which relation reads

$$\frac{\rho_0 V_{c0}}{\gamma\, p_{c0}}\, \Delta\dot{P} \;+\; \alpha\, \Delta P = w A_c\, \dot{\tau}, \tag{9}$$

where ρ_0 is the ambient air density in the chambers, V_{c0} the initial air volume in each reservoir, p_{c0} the ambient air pressure, $\gamma = 1.4$ the specific heat ratio for an adiabatic process, and A_c the cross-sectional area of each reservoir. The torque acting on the water column due to the air pressure difference is defined as

$$T_{air} = -wA_c. \tag{10}$$

Now, the dynamic behaviour of the entire WEC system can therefore be expressed in compact matrix form as shown in Eq. (11):

$$[\boldsymbol{M}_{in} + \boldsymbol{A}(\omega)]\ddot{\boldsymbol{q}} + [\boldsymbol{C} + \boldsymbol{B}](\omega)\dot{\boldsymbol{q}} + [\boldsymbol{K} + \boldsymbol{K}_h]\boldsymbol{q} = a_w(\omega)\boldsymbol{F}_{exc}(j\omega), \tag{11}$$

where the state vector $\boldsymbol{q} \in \mathbb{R}^8$ is

$$\boldsymbol{q} = [x, y, z, \gamma, \delta, \psi, \tau, \Delta P]^T, \tag{12}$$

and the mass matrix $\boldsymbol{M} \in \mathbb{R}^{8\times8}$, the damping matrix $\boldsymbol{C} \in \mathbb{R}^{8\times8}$, and the stiffness matrix $\boldsymbol{K} \in \mathbb{R}^{8\times8}$ are fulfilled respectively as:

$$\boldsymbol{M} = \begin{bmatrix} m_{\text{tot}} & 0 & 0 & 0 & 0 & 0 & -a_{1\tau} & 0 \\ 0 & m_{\text{tot}} & 0 & 0 & 0 & 0 & 0 & 0 \\ 0 & 0 & m_{\text{tot}} & 0 & 0 & 0 & 0 & 0 \\ 0 & 0 & 0 & I_{xx} & I_{xy} & I_{xz} & 0 & 0 \\ 0 & 0 & 0 & I_{yx} & I_{yy} & I_{yz} & a_{5\tau} & 0 \\ 0 & 0 & 0 & I_{zx} & I_{zy} & I_{zz} & 0 & 0 \\ -a_{\tau 1} & 0 & 0 & 0 & a_{\tau 5} & 0 & a_{\tau\tau} & 0 \\ 0 & 0 & 0 & 0 & 0 & 0 & 0 & 0 \end{bmatrix}, \tag{13}$$

$$\boldsymbol{C} = \begin{bmatrix} 0 & 0 & 0 & 0 & 0 & 0 & 0 & 0 \\ 0 & 0 & 0 & 0 & 0 & 0 & 0 & 0 \\ 0 & 0 & 0 & 0 & 0 & 0 & 0 & 0 \\ 0 & 0 & 0 & 0 & 0 & 0 & 0 & 0 \\ 0 & 0 & 0 & 0 & 0 & 0 & 0 & 0 \\ 0 & 0 & 0 & 0 & 0 & 0 & 0 & 0 \\ 0 & 0 & 0 & 0 & 0 & 0 & b_{\tau\tau} & wA_c \\ 0 & 0 & 0 & 0 & 0 & 0 & -wA_c & \frac{\rho_0 V_{c0}}{\gamma p_{c0}} \end{bmatrix}, \tag{14}$$

$$\boldsymbol{K} = \begin{bmatrix} 0 & 0 & 0 & 0 & 0 & 0 & 0 & 0 \\ 0 & 0 & 0 & 0 & 0 & 0 & 0 & 0 \\ 0 & 0 & 0 & 0 & 0 & 0 & 0 & 0 \\ 0 & 0 & 0 & 0 & 0 & 0 & 0 & 0 \\ 0 & 0 & 0 & 0 & 0 & 0 & c_{5\tau} & 0 \\ 0 & 0 & 0 & 0 & 0 & 0 & 0 & 0 \\ 0 & 0 & 0 & 0 & c_{\tau 5} & 0 & c_{\tau\tau} & 0 \\ 0 & 0 & 0 & 0 & 0 & 0 & 0 & \alpha \end{bmatrix}. \tag{15}$$

Following [30], under the frequency-domain assumptions, for a single degree of freedom, the desired input–output response can be calculated as transfer functions $H(j\omega)$ reading

$$\frac{q(j\omega)}{f(j\omega)} = \frac{1}{-\omega^2 M + j\omega B + K}, \tag{16a}$$

$$G(j\omega) = j\omega\, H(j\omega). \tag{16b}$$

where $f(j\omega)$ and $q(j\omega)$ denote the Fourier transforms of $f(t)$ and $q(t)$, and $H, G : \mathbb{C} \mapsto \mathbb{C}$, $j\omega \mapsto H(j\omega), G(j\omega)$ are the corresponding input–output operators.

Considering that the excitation force $f(t)$ is modelled as a stationary Gaussian process (*i.e.* as for the wave elevation in our case) characterised by its power spectral density (PSD) $S_{ff} : \mathbb{R}^+ \mapsto \mathbb{R}^+$, $\omega \mapsto S_{ff}(\omega)$ the PSD from the wave elevation $S_{\eta\eta}(\omega)$ is calculated through the excitation operator $E(j\omega)$, which accounts for Froude–Krylov and diffraction effects [32], namely

$$S_{ff}(\omega) = |E(j\omega)|^2 S_{\eta\eta}(\omega). \tag{17}$$

The response PSDs for displacement and velocity of the WEC, $S_{qq}(\omega)$ and $S_{\dot{q}\dot{q}}(\omega)$, then follow from

$$S_{qq}(\omega) = |H(j\omega)|^2 S_{ff}(\omega), \tag{18a}$$

$$S_{\dot{q}\dot{q}}(\omega) = |G(j\omega)|^2 S_{ff}(\omega). \tag{18b}$$

Although written here for a single DoF system, these relations can be straightforwardly extended to multi-DoF models.

Assuming that $f(t)$ has zero mean, the variance of the displacement response $q(t)$ is fully described by the zero-order spectral moment $m_q \in \mathbb{R}^+$ [37],

$$m_q = \int_0^\infty S_{qq}(\omega)\, \mathrm{d}\omega, \tag{19}$$

which provides a complete probabilistic characterisation of the Gaussian response. For a single-DoF system, the probability density function (PDF) of q, denoted $f_q : \mathbb{R} \mapsto \mathbb{R}$, is then

$$f_q(q) = \frac{1}{\sqrt{2\pi m_q}} e^{\left(-\frac{q^2}{2m_q}\right)}. \tag{20}$$

Therefore, for the described WEC object of the current investigation, the transfer function between wave elevation and system response, namely $H(j\omega)$, can now be formulated and reads

$$H(j\omega) = \frac{\boldsymbol{F}_{exc}(j\omega)}{-\left[\boldsymbol{M} + \boldsymbol{A}(\omega)\right]\omega^2 + \left[\boldsymbol{C} + \boldsymbol{B}(\omega)\right]j\omega + \left[\boldsymbol{K} + \boldsymbol{K}_h\right]}, \tag{21}$$

and the output PSD of the state vector of the WEC ($S_{qq}(\omega)$) is

$$S_{qq}(\omega) = \left|H(j\omega)\right|^2 S_{\eta\eta}(\omega). \tag{22}$$

Finally, the zero-order moment σ_q standard deviation (rms value) of the response is obtained as

$$\sigma_q = \sqrt{\int_0^\infty S_q(\omega)\, d\omega}, \tag{23}$$

Under the linear-orifice assumption, and considering that ΔP is a zero-mean Gaussian process, the mean pneumatic gross power $\bar{P}$ is given by

$$\bar{P} = \frac{\alpha}{\rho_0}\sigma_{\Delta P}^2. \tag{24}$$

In conclusion, the gross AEP for a given site is evaluated following:

$$AEP_{\text{gross}} = \frac{3600 \cdot 24 \cdot 365}{100} \sum_{i=1}^{N_o} \text{Occ}_{\%}^i \bar{P}^i, \tag{25}$$

where the N_o sea states with non-zero occurrence $\text{Occ}_{\%}^i$ are spanned, and $\bar{P}^i$ denotes the mean net power associated with each ith sea state.

It is worth remarking that the numerical framework adopted in this work is intended as a preliminary, physics-based tool for techno-economic optimisation and comparative site assessment of an early-stage WEC concept. Nevertheless, the proposed numerical framework is grounded in consolidated mathematical models that are well established in the literature, namely linear potential-flow hydrodynamics, solved here through NEMOH, and a lumped-parameter representation of the U-tank dynamics. Moreover, these modelling approaches are supported by prior experimental investigations on case studies that are representative of, and in several aspects equivalent to, those addressed in the present work. Interested readers can refer to [38] for an experimental study concerning the hull hydrodynamics and to [35] for others coping with the U-tank dynamics.

The above assumptions are considered appropriate for a preliminary design-stage assessment under representative operational sea states, which are the most relevant for AEP estimation. Conversely, under extreme conditions, nonlinear effects may become important and are expected to be addressed in subsequent higher-fidelity design stages.

2.2. Design parameterisation

To conduct a techno-economic analysis and subsequently optimise the design of the system investigated in the present work, a parameterisation of the device is necessary. Similarly to previous works [22], the WEC inertial and geometrical properties are univocally described

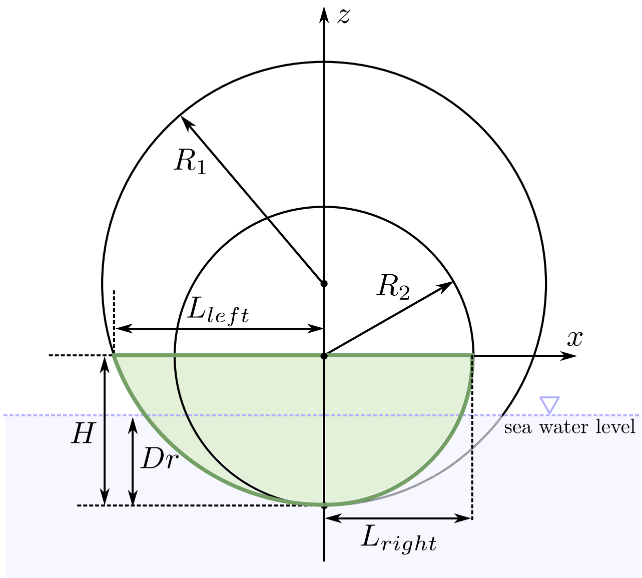

Fig. 3. U-WEC's hull parametrisation.

by means of 10 design variables, *i.e.* 5 for the hull and 5 for the U-tank-Wells unit.

The hull's overall dimensions are length L, width W, and height H along the x-, y-, and z-axes, respectively, as shown in Fig. 3. It is formed by extruding a profile defined in the x-z plane along the y axis and is symmetric about the x-z plane. The hull's profile is defined by two non-dimensional geometric parameters: the shape ratio h and the height ratio k:

- Shape ratio, $h = \frac{\text{right-semi length}}{L}$, $0 < h < 1$. This parameter controls fore-aft asymmetry: $h = 0.5$ yields a profile symmetric about the y-z plane, while values $h < 0.5$ or $h > 0.5$ shift the hull's volume towards the bow or stern, respectively.
- Height ratio, $k = \frac{H}{\min[hL, (1-h)L]}$. This parameter relates the vertical to the longitudinal scale of the floater.

Once the parameters L, h, and k are specified, the hull's profile in the x-z plane is generated by two circular arcs whose points satisfy the following geometric constraints:

- the centres of the two circles have the same x-coordinates,
- the circle C_1 is constrained to pass exactly through the point $(-L_{\text{left}}, 0)$, and the circle C_2 through the point $(L_{\text{right}}, 0)$. Both circles also intersect at the keel point $(0, -H)$ where they meet tangentially.

Together, these constraints fully determine each circle's centre $(0, z_C)$ and radius R, namely:

$$z_C = \frac{L_{\text{side}}^2 - H^2}{2H}, \tag{26a}$$

$$R = \frac{L_{\text{side}}^2 + H^2}{2H}, \tag{26b}$$

where $L_{\text{side}} = L_{\text{left}}$ or $L_{\text{side}} = L_{\text{right}}$ for the left and right arcs, respectively.

Another key hull design parameter is the draft ratio α, defined as the ratio of the hull's draft D_r to its overall height H. Once the hull geometry and draft are established, the device's displacement mass can be calculated. The structural mass of the hull m_h is estimated using the empirical relation $m_h = 0.09\, LWH(t)$ [22] based on previous experience with the ISWEC and PeWEC devices. For inertia-matrix calculations, the hull is modelled as having walls of equivalent thickness, simplifying the geometry while preserving its mass distribution. The hull is assumed to be made of steel with a density of $7800\ \text{kg/m}^3$, while the ballast is made of concrete with a density of $2200\ \text{kg/m}^3$. The ballast compartments are positioned at the bow and stern. The ballast mass is then determined by subtracting the hull mass and the U-tank mass from the total displacement mass.

The U-tank parametrisation begins with the U-tank mass ratio U_m, defined as the mass of water contained in the U-tank divided by the system's total displacement mass. It is also assumed that the U-tank's midline is aligned with the device's centre of gravity (CoG) along the vertical z-axis. The U-tank length ratio is defined as the ratio between the U-tank's maximum lateral extent L_{tot} along the y-axis and the maximum lateral space available inside the hull, as bounded by the ballast compartment walls. The U-tank height ratio H_r is defined as the ratio of the water depth h_r within the reservoirs to their maximum height h_t. Finally, the reservoir width ratio W_r and duct width ratio H_d are defined, respectively, as the reservoir's width w_r and the central duct's width h_d each divided by the water level height h_r. Once the U-tank design parameters are uniquely defined, the U-tank's geometry and inertial properties can be determined.

In conclusion, the WEC device can be completely defined by the described set of 10 design variables, *i.e.* $N_d = 10$.

2.3. Numerical modelling and design of the Wells turbine

After identifying the optimal hull and U-tank configurations, the Wells turbine is tailored to each device's operating conditions and its real performance curve is used to recalculate energy output. This work therefore, implements a two-stage optimisation: in Stage 1, hull and U tank parameters are defined using a simplified turbine model; in Stage 2, the specific the Wells turbine design that maximises the energy production is selected.

In this study, we developed a computational framework to generate and evaluate a broad set of Wells turbine designs tailored to specific device and metocean conditions. The design procedure is based on the Wells design theory proposed by Raghunathan [39]. The process begins with the initialisation of fluid properties, including atmospheric pressure p_{atm}, air density ρ, and dynamic viscosity μ. A design space is then established, spanning a practical range of blade counts n_b, tip diameters D_{tip}, hub-to-tip diameter ratios h, rotational speeds ω, solidity values σ, and NACA airfoil profiles.

Discrete flow rate and pressure profiles are generated to span the full range of expected operating conditions. The algorithm systematically evaluates turbine geometries by computing hub and tip velocities, from which the local angles of attack at the blade hub and tip are derived. Configurations are filtered based on these angles of attack: candidates are discarded if the angle at the hub exceeds a maximum threshold (to avoid stall) or if the angle at the tip falls below a minimum value (indicating ineffective energy extraction). This pre-screening ensures that only aerodynamically viable machines are considered. The adopted values, ranges and parameters for the design algorithm in the specific case study are presented in Table 1. Fig. 4 shows an example of generated Wells turbine geometry.

For each turbine configuration, defined by $d_w = [n_b, D_{\text{tip}}, h, \omega_w, \sigma, \text{NACA}]$, a blade element analysis is conducted across n_r radial sections of the rotor for all feasible configurations that survived the pre-screening. As output, a single Wells turbine is described by its design parameters d_w and the corresponding non-dimensional coefficients $o_w = [\phi, \pi, \psi, \eta]$, defined as:

$$\pi = \frac{P_{\text{total}}}{\rho\, \omega_w^3 D^5}, \tag{27a}$$

$$\phi = \frac{Q}{\omega_w D_{\text{tip}}^3}, \tag{27b}$$

$$\psi = \frac{\Delta P}{\rho\, \omega_w^2 D^2}, \tag{27c}$$

Table 1
Input conditions, design parameters, and constraints used for the Wells turbine optimisation.

Category	Parameter	Unit	Value/range
Physical properties	Atmospheric pressure p_{atm}	Pa	101 325
	Air density ρ	kg/m^3	1.225
	Dynamic viscosity μ	Pa·s	1.81×10^{-5}
Design parameters	Blade count n_b	–	5 : 1 : 10
	Tip diameter D_{tip}	m	0.5 : 0.5 : 3
	Angular velocity ω_w	rad/s	15 : 10 : 315
	Hub-to-tip ratio h	–	0.65 : 0.05 : 0.85
	Solidity σ	–	0.5 : 0.1 : 0.8
	NACA airfoils	–	0015-0022
	Radial sections n_r	–	3
	Flow rate discretisation	m^3/s	20 values from 0 to Q_{max}
	Pressure drop discretisation	Pa	20 values from 0 to ΔP_{max}
	Number of Wells turbine in parallel	–	5, 10
	Reynolds number range	–	10^5 to 10^7
	Angle of attack range	deg	−10 : 1 : 24

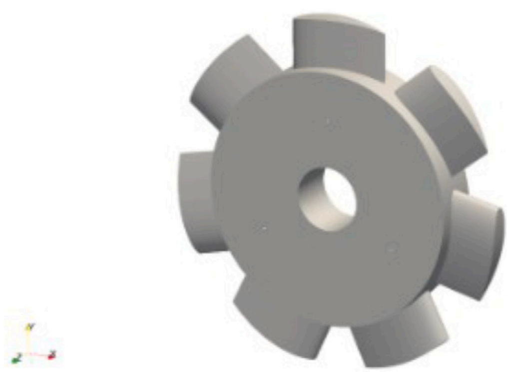

Fig. 4. Example of a generated Wells turbine geometry.

$$\eta = \frac{\pi}{\phi\,\psi}. \tag{27d}$$

Since the relationship between the non-dimensional flow coefficient ϕ and pressure coefficient ψ is almost linear in operational conditions, it can be write [40]:

$$\phi = K_t\,\psi, \tag{28}$$

K_t is a proportionality constant depending on turbine geometry. Eq. (8) can therefore be reformulated as:

$$\dot{m} = \frac{K_t D}{\omega_w}, \tag{29}$$

where the discharge coefficient α now depends explicitly on the Wells turbine's geometry and its angular speed ω_w. By employing a dedicated control system for the electrical generator connected to the turbine, the angular velocity ω_w can be optimised for each sea state within its operational limits to maximise power extraction. The instantaneous power output of the turbine can be calculated following:

$$P_t = \rho\,\omega_w^3 D^5 \pi = \rho\,\omega_w^3 D^5 f_P\left(\frac{p}{\rho\,\omega_w^2 D^2}\right). \tag{30}$$

Since $p(t)$ follows a Gaussian distribution with variance σ_p^2 given by Eq. (23), the turbine's average power output can be determined by:

$$\bar{P}_t = \frac{\rho\,\omega_w^3 D^5}{\sqrt{2\pi}\,\sigma_p}\int_{-\infty}^{+\infty}\exp\left(-\frac{p^2}{2\sigma_p^2}\right) f_P\left(\frac{p}{\rho\,\omega_w^2 D^2}\right)\mathrm{d}p. \tag{31}$$

Accordingly, one can compute the non-dimensional average power output of the turbine:

$$\bar{\pi} = \frac{1}{\sqrt{2\pi}\,\sigma_\psi}\int_{-\infty}^{+\infty}\exp\left(-\frac{\psi^2}{2\sigma_\psi^2}\right) f_P(\psi)\,\mathrm{d}\psi, \tag{32a}$$

$$\sigma_\psi = \frac{\sigma_p}{\rho\,\omega_w^2 D^2}. \tag{32b}$$

Therefore, once the non-dimensional average power output $\bar{\pi}$ is determined the average power output $\bar{P}_t$ and average efficiency $\bar{\eta}$ can be calculated as:

$$\bar{P}_t = \bar{\pi}\,\rho\,\omega_w^3 D^5, \tag{33a}$$

$$\bar{\eta} = \frac{\bar{\pi}}{K_t \sigma_\psi^2}. \tag{33b}$$

It is worth noting that the present Wells turbine framework focuses on aerodynamic performance within a preliminary assessment; material durability aspects will require attention in subsequent design stages. Real-scale OWC experience, such as that of the Pico Power Plant, has highlighted pitting corrosion and erosion-corrosion as key degradation mechanisms [41]. Notably, the sealed hull of the U-WEC reduces direct exposure to sea spray and saline atmosphere, potentially improving turbine durability compared to conventional nearshore OWC installations.

3. Case studies

Wave energy converters are highly site-specific: local metocean conditions profoundly shape device design and performance. Selecting the right location is therefore crucial for achieving successful system optimisation. This study focuses on two sites with distinct wave climates, represented in Fig. 5. The first, in the Strait of Sicily (CDS), lies beside a major offshore wind development zone (*e.g.* see [42]), offering opportunities for shared infrastructure and cost savings, and ranks among the Mediterranean's most energetic wave power sites. The second is the European Marine Energy Centre (EMEC) in Scotland, which exemplifies the high-energy wave characteristic of northern Europe.

Wave data for the EMEC [43] site are publicly available, whereas the wave climate at the Strait of Sicily was characterised using high-resolution reanalysis data from the Copernicus Marine Service [44]. The wave occurrences scatters at both sites, used for the AEP assessment, are shown in Fig. 6 as a function of significant wave height H_s and energetic period T_e, while their cumulative distribution with respect to T_e are reported in Fig. 7. Table 2 summarises the most occurrent sea state parameters and annual power density for both sites, highlighting that the Northern European location offers a substantially higher energy resource than the Mediterranean. The metocean data reveal a clear shift towards longer wave periods at the EMEC site.

3.1. Techno-economic optimisation framework

As discussed, for a given set d of the 10 design variables, the techno-economic tool first determines the device's geometry and inertial properties, then computes its hydrodynamic coefficients using

Fig. 5. Satellite view of the site in the Mediterranean Sea and in north Europe.

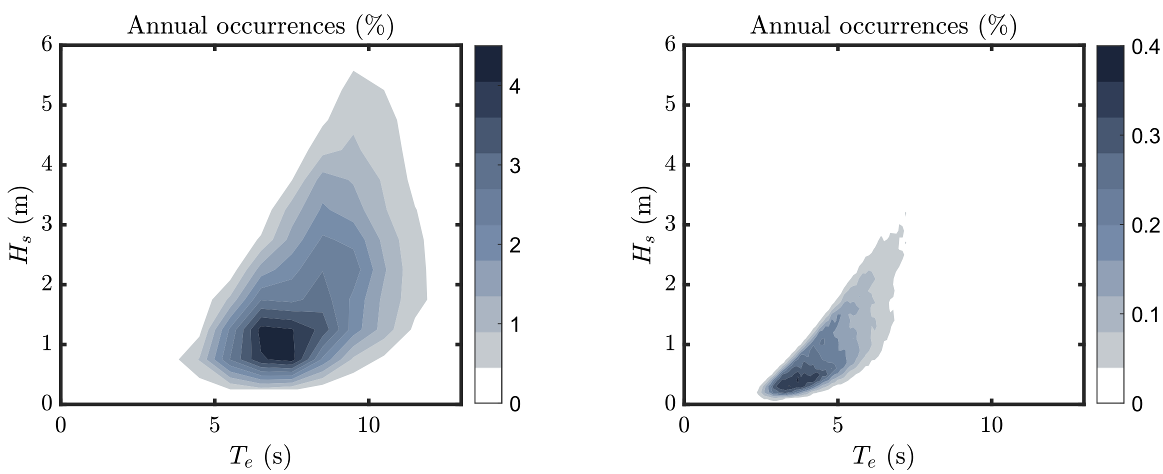

Fig. 6. Wave occurrences scatter matrix for the EMEC site in north Europe (left) and for the Strait of Sicily site in the Mediterranean Sea (right).

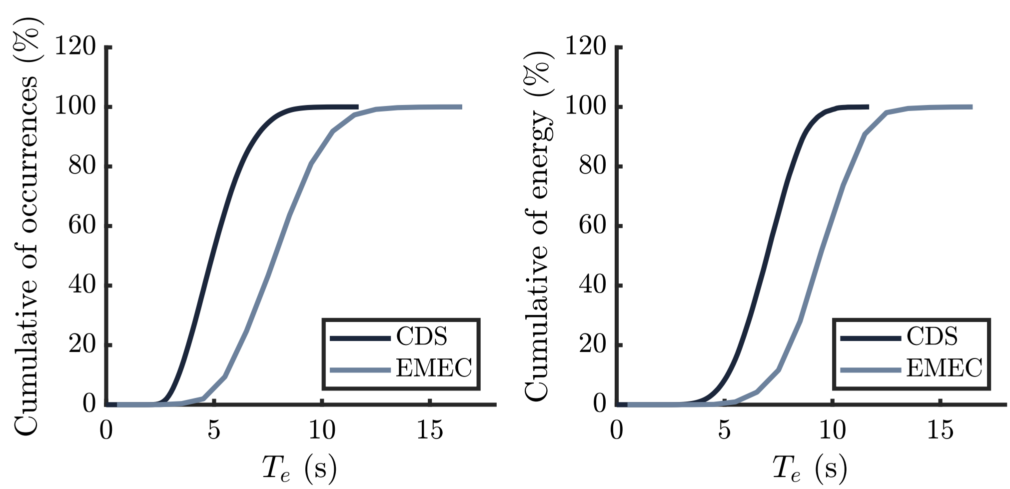

Fig. 7. Cumulative distribution of occurrences (left) and energy (right) as function of energetic period T_e for the two sites.

the BEM solver NEMOH. Once the full system transfer function is obtained, simulations are carried out for each sea state, and the mean power output of an ideal Wells turbine is maximised by optimising the linear discharge coefficient α. Finally, the AEP_{gross} is calculated by combining the optimised power matrix with the metocean occurrence scatter table for the installation site. The techno-economic optimisation of the U-tank WEC system employs a multi-objective framework, targeting two goals previously described in Section 2: maximising the device's AEP_{gross} at the chosen installation site, and minimising its displacement mass.

Table 2
Most occurrent sea state parameters and power density for the two sites under analysis.

Parameter	Unit	EMEC	CDS
Most occurrent energetic period - T_e^*	(s)	8.50	4.60
Most occurrent significant wave height - H_s^*	(m)	1.25	0.50
Wave power density - P_w	(kW/m)	32.40	7.40

Table 3
Exploration space of the U-WEC's design variables used in the optimisation framework.

Parameter	Unit	D_l	D_u
Hull length - L	(m)	10	35
Hull width - W	(m)	7	25
Hull shape ratio - h	(/)	0.1	0.9
Hull height ratio - k	(/)	0.3	1
Hull draft parameter - α	(/)	0.65	0.85
U-tank mass ratio - U_m	(/)	0.1	0.4
U-tank length ratio - L_r	(/)	0.4	1
U-tank height ratio - H_r	(/)	0.3	0.6
U-tank's reservoir width ratio - W_r	(/)	0.1	0.5
U-tank's duct height ratio - H_d	(/)	0.1	0.5

To solve the multi-objective optimisation problem, the Non-dominated Sorting Genetic Algorithm II (NSGA-II) [45] has been adopted. Indeed, the use of a metaheuristic algorithm, such as GA, is a widely adopted framework in the literature [46]. The choice was motivated by the fact that the present design problem is simulation-based (*i.e.* not describable with an LP or NLP formulation), constrained, nonlinear, and potentially non-convex. In this context, NSGA-II represents a robust and widely used baseline algorithm, capable of combining convergence pressure and diversity preservation through elitist non-dominated sorting and crowding-distance mechanisms. In the present implementation, the optimisation was carried out through MATLAB's `gamultiobj` routine, using a population size of 70 individuals and 150 generations. Moreover, the use of a GA also allows us to easily implement parallelisation techniques, increasing computational efficiency of the optimisation algorithm. For the present study, a cluster that allowed all individuals in each generation to be processed in parallel (*i.e.* utilising 70 cores) has been employed. The regularity of the resulting Pareto fronts and the consistency of the associated design trends indicate that the adopted optimisation settings provided satisfactory practical convergence for the exploratory scope of the present study.

Table 3 provides an overview of the exploration space adopted for the optimisation of the U-WEC. The bounds reported in Table 3 were selected on the basis of previous design experience on related WEC configurations (see, *e.g.* [22]), together with geometric-feasibility and practical design considerations related to manufacturability constraints. Accordingly, the following optimisation results should be interpreted as optimal within the adopted exploration space. Different admissible ranges could lead to partly different Pareto-optimal solutions, especially for variables whose optimal values approach the imposed bounds.

4. Results

4.1. Techno-economic optimisation results

Unlike earlier work on this WEC concept [17], which targeted a single performance metric (*e.g.* hydrodynamic efficiency or average annual power) with only a small set of adjustable geometric variables, the present approach parametrises multiple hull and U-tank geometries within a true bi-objective framework, maximising AEP_{gross} while minimising displacement mass. By co-optimising the U-tank and hull system, with sloshing and pitch resonances tuned in concert, energy capture can be enhanced. Parallel optimisations across two contrasting

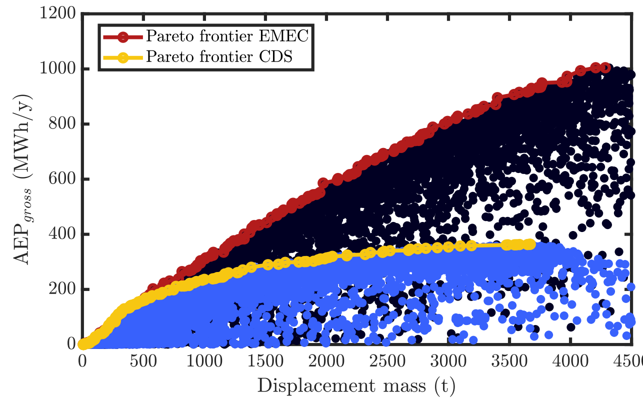

Fig. 8. Techno-economic optimisation results showing displacement mass versus AEP_{gross} for both sites, with the respective Pareto fronts highlighted.

wave climates demonstrate how site-specific conditions reshape the Pareto frontier and reveal the key techno-economic drivers.

Fig. 8 presents the optimisation results, with EMEC's Pareto front shown in red and the Strait of Sicily's (CDS) in yellow. As expected from the wave climate characterisation, EMEC achieves substantially higher AEP but requires larger displacement masses, reflecting higher capital costs. At low values of displacement mass, the two fronts overlap, indicating similar device performance. Beyond that intersection, the Northern Europe site consistently outperforms the Mediterranean site, producing up to three times the AEP_{gross} for the same displacement mass. The higher gross productivity observed at EMEC is supported by richer wave resource. These oceanic conditions, as seen in the following analysis, also favour optimal hull and U-tank configurations with longer natural periods, thereby improving resonance matching with the local wave climate. However, this does not necessarily imply a uniformly higher normalised conversion efficiency. From an interpretation standpoint, the present comparison is intended as an internally consistent assessment of the same U-WEC concept under two contrasting wave climates, rather than as a fully general benchmark across different technologies or perfectly identical environmental scenarios. Therefore, the main value of the analysis lies in showing how local metocean conditions influence the techno-economic optimum, *i.e.* the Pareto-front shape, and the associated design drivers.

The analysis is then extended towards the investigation of the principal trends concerning the design variables for the WECs composing the Pareto set, investigating both the WEC's hull and the U-tank across the two sites. Clear patterns emerged from the optimisation results, depicted in Fig. 9. An evident trend is that for the same displacement, EMEC optimised hulls are longer and narrower than those for the Strait of Sicily. This reflects the need to increase pitch inertia, and thus the device's resonant period, to better match longer ocean waves. The hull shape ratio consistently converges to an asymmetric value of approximately 0.3, suggesting that pronounced hull asymmetry enhances hydrodynamic conversion efficiency (see Fig. 9). A possible physical interpretation to this outcomes is that hull asymmetry improves the way in which incident-wave loads are channelled into the coupled hull motions that excite the U-tank (*e.g.* maybe increasing the heave-pitch coupling effects), thereby favouring power generation. Indeed, an asymmetric configuration is consistent with famous WECs design configuration, such as the Salter's duck [47] and the UGEN device [17]. Moreover, every Pareto-optimal configuration aligns the U-tank's sloshing period with the hull's natural resonance, underscoring the pivotal role of sloshing tuning in overall system performance. Although absolute energy production is higher at EMEC, the relative capture width (RCW) is greater at the Mediterranean site because more compact hulls can still deliver strong conversion efficiency in the presence of moderate length waves.

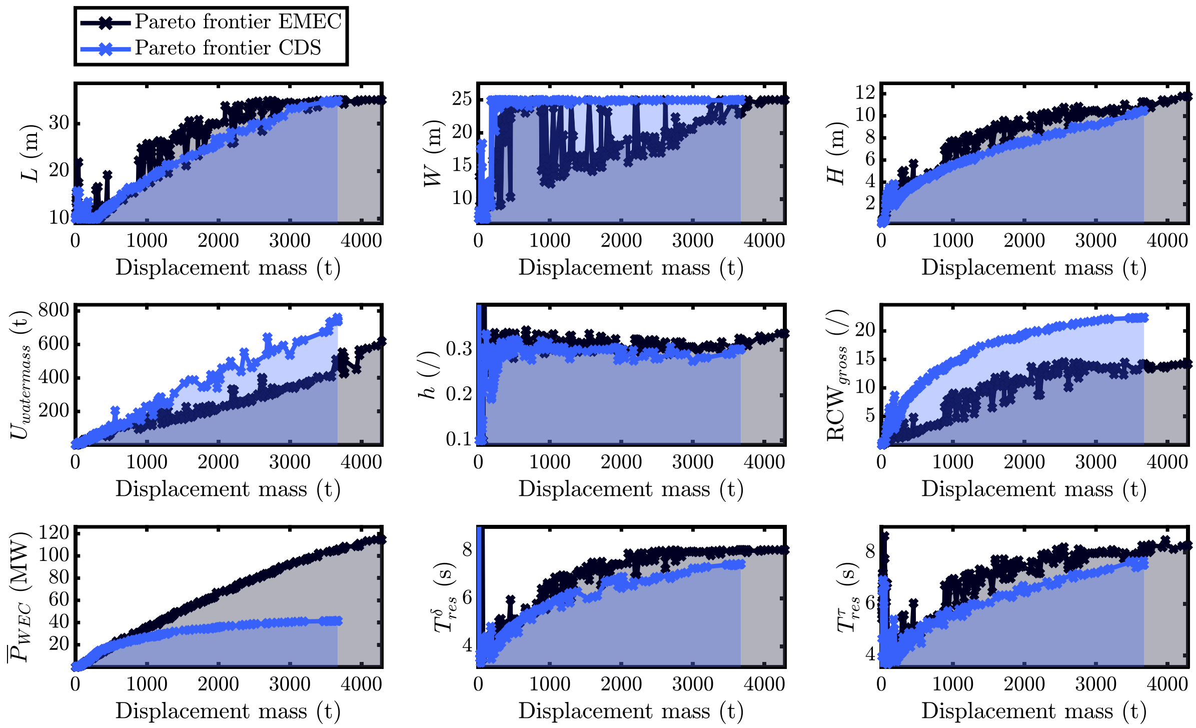

Fig. 9. Design variables trends for the EMEC and CDS devices of the Pareto set.

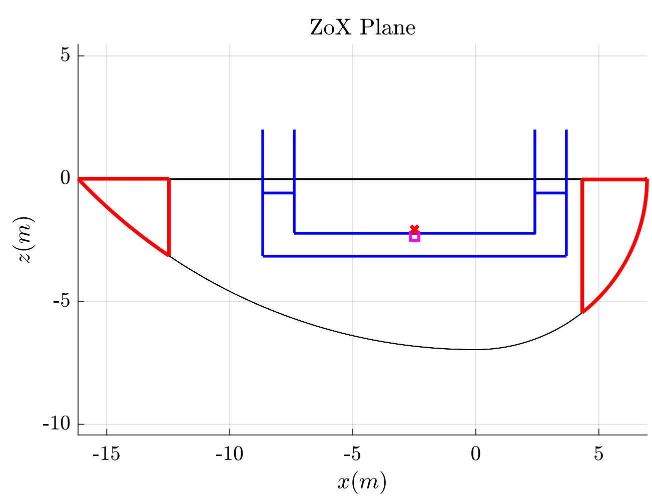

Fig. 10. Optimal hull profile for the Mediterranean Sea L-CDS with the hull shown in black, the ballast in red and the U tank in blue; magenta marker indicates the U-Tank CoG and red marker indicates the overall device CoG.

Table 4
Techno-economic parameters of the optimal devices selected.

Parameter	Unit	S-CDS	L-CDS	L-EMEC
Displacement	t	500	1600	1600
Gross AEP	MWh/y	169	291	481
Gross RCW	%	10.5	18	10.3
Gross Average Power	kW	19.2	33.2	55
Hull length	m	13.1	23.1	27.8
Hull width	m	24.5	24.9	16.5
Hull height	m	5	7	8.8
Draft	m	2.6	4.5	6.7
Pitch resonance period	s	4.9	6	7.2
Hull structural mass	t	116	360	364
Ballast mass	t	292	854	1070
Utank water mass	t	92.4	387	166
Utank resonance period	t	4.9	6.2	7.4

These results confirm that optimal configurations are inherently wave-climate-dependent: a device optimised for Mediterranean conditions would be off-resonant and suboptimal if deployed in a higher-energy, longer-period environment without re-optimisation. The proposed framework, however, is general and applicable to any site with available metocean data.

4.2. Analysis of the optimal devices and Wells turbine selection

Rather than relying on a fixed, non-optimised Wells turbine, this study actively tunes turbine geometry to match each WEC's dynamic behaviour, thereby maximising efficiency on every layout and explicitly assessing how site and device parameters shape turbine performance and characteristics. To evaluate how device size and site affect Wells turbine design and overall energy output, three devices have been selected for comparison (see Table 4). At the Mediterranean site a small size device with 500 t displacement (S-CDS) and a large size device with 1600 t displacement (L-CDS) were chosen. At the oceanic site a large size device with the same 1600 t (L-EMEC) displacement has been selected for comparison.

As highlighted, each device differs in both geometric characteristics and power generation capacity. The aim is therefore to identify the optimal Wells turbine geometry for each device and to understand how device and site climate influence that optimal design and its expected performance. Fig. 10 shows the optimal large size hull geometry for the Mediterranean site (L-CDS), showing that the optimisation converged on an asymmetric hull profile to enhance system performance.

Fig. 11 compares the surge, heave, and pitch RAOs of the three selected optimal hull configurations (S-CDS, L-CDS, and L-EMEC). The results show a systematic shift of the dominant resonance peaks towards longer wave periods as hull size increases and geometry is modified.

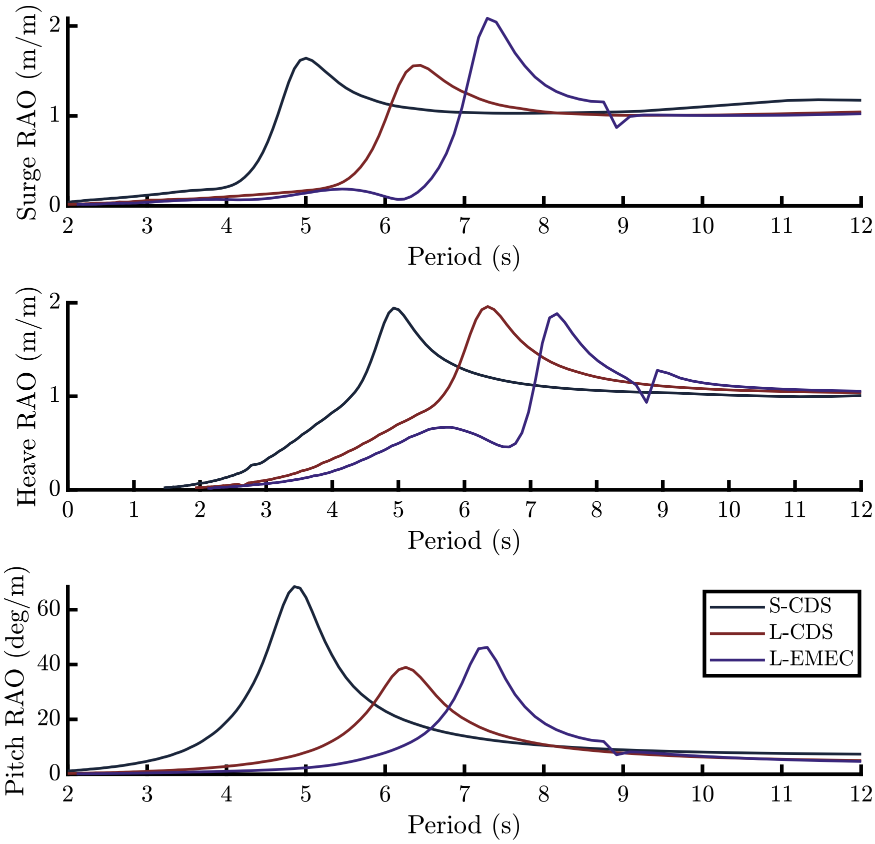

Fig. 11. Comparison of the surge, heave, and pitch response amplitude operators (RAOs) of the three selected optimal hulls.

The shift in RAO peaks is governed by the increase in pitch moment of inertia with hull length, which lowers the system natural frequency, causing larger configurations to resonate with longer-period waves.

The S-CDS configuration exhibits its main resonances around 5 s, particularly in pitch, indicating a stronger interaction with short-period waves typical of Mediterranean wave climates. The L-CDS hull presents smoother responses with resonances occurring at intermediate periods (approximately 6–6.5 s), representing a balanced dynamic behaviour. In contrast, the L-EMEC configuration shows pronounced resonant responses at longer periods (around 7–7.5 s), making it more suitable for oceanic environments dominated by long-period swell.

Table 5 presents the optimal Wells turbine designs for the three devices, while Fig. 12 compares their non-dimensional average power output and efficiency curves. For large size devices, L-CDS and L-EMEC, the optimisation selected turbines with the same characteristics. By contrast, the small size device, S-CDS, requires a turbine with similar geometry, but with a smaller diameter and a higher nominal speed. This difference reflects the lower flow rate and pressure in the smaller device's U-Tank, making a more compact turbine necessary to ensure proper operation under those conditions.

Consistently with the RAO trends discussed in Fig. 11, the mean power production matrices and the RCW shown in Fig. 13 reflect the shift of the dominant resonant periods among the three hull configurations. The highest efficiency, reaching values of approximately 30%, is observed for the S-CDS device under resonant conditions at energy periods around 4–5 s, indicating that this configuration is particularly well suited to short-period waves typical of Mediterranean wave climates.

Table 5
Design parameters of the optimal Wells turbines.

Parameter	Unit	S-CDS	L-CDS	L-EMEC
Number of Wells turbine	–	10	10	10
NACA profile	–	17	15	15
Diameter at the tip	m	1	1.5	1.5
Nominal speed	rpm	1100	811	811
Number of blades	–	5	5	5
Solidity	–	0.8	0.6	0.6
Hub to tip ratio	–	0.85	0.85	0.85
K_t	–	0.1	0.059	0.059
Rated Power	kW	80	300	300
Gross AEP	MWh/y	142	257	388
Net AEP	MWh/y	113	187	282
Net RCW	%	7.1	11.6	6
Aerodynamic efficiency	%	79	72	72

4.3. Performance analysis across selected Italian offshore sites

This section analyses the system performance in terms of energy productivity and efficiency for the two optimal hull sizes designed for Mediterranean conditions and optimised for the Strait of Sicily site, when applied to several offshore locations of high interest in Italy. Fig. 14 reports the six sites selected for the analysis. Three locations were chosen due to their relevance for potential co-location with offshore wind developments, namely the Strait of Sicily, North-West Sardinia, and South-East Apulia, which are currently the subject of offshore wind project proposals [48]. The remaining three sites (Ustica, Ponza, and Gorgona) represent off-grid island contexts that still rely heavily on fossil fuels, where marine renewable energy could play a key role in supporting the energy transition of Italian islands.

The wave resource characteristics of the selected sites are also reported in Table 6, highlighting a marked heterogeneity across locations. In particular, the wave power density varies from the least energetic site in South-East Apulia (3.10 kW/m) to the most energetic site in

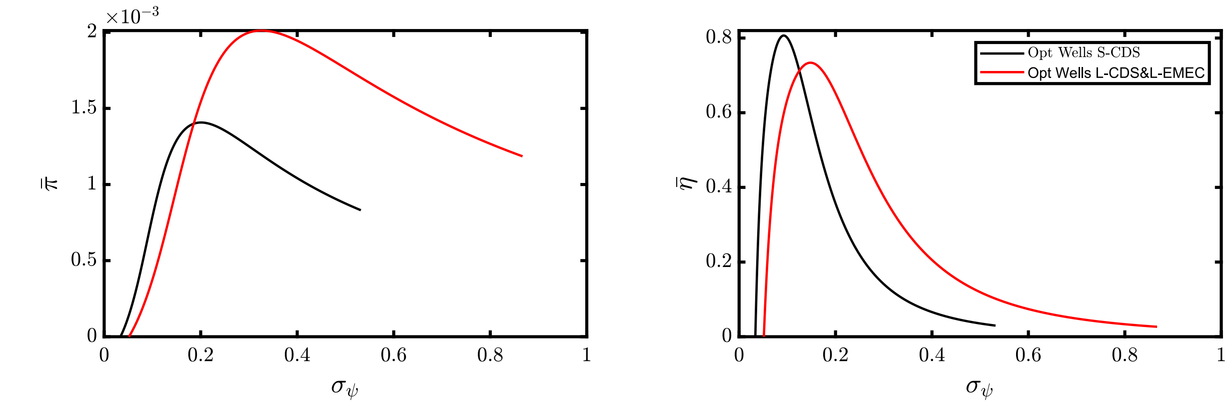

Fig. 12. The left-hand plot shows the non-dimensional average power output coefficient curve, while the right-hand plot shows the non-dimensional average efficiency curves for the two optimal Wells turbines identified.

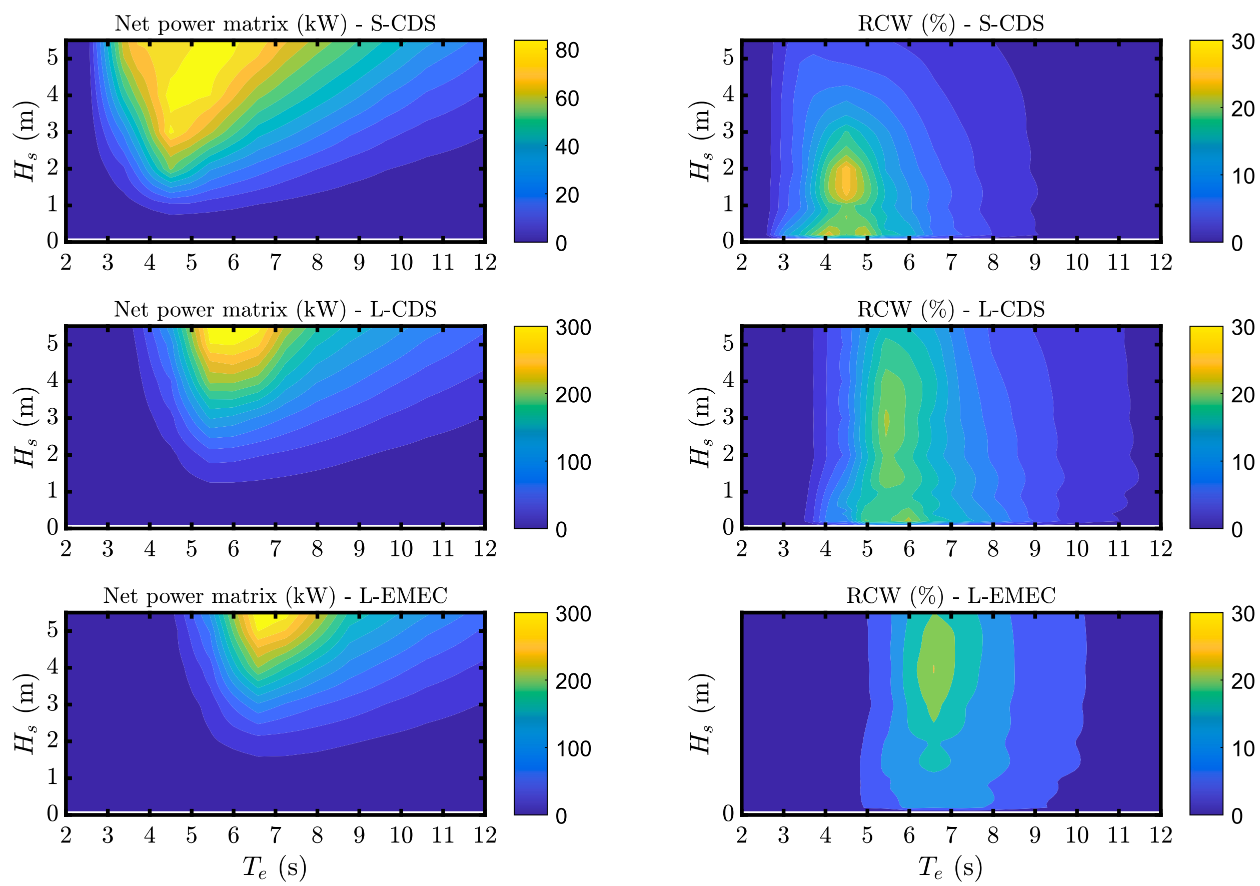

Fig. 13. Comparison of the mean power production matrices and RCW for the three selected optimal hulls.

North-West Sardinia (9.75 kW/m), providing a representative range of Mediterranean wave conditions for assessing system performance.

Table 7 reports the values of annual energy production (AEP) and RCW for the two optimal devices evaluated at the six analysed sites. It is worth noting that the higher efficiency is consistently achieved by the larger L-CDS hull, as its resonance period is closer to the most energetic wave conditions characterising these locations. Moreover, the site exhibiting the highest RCW corresponds to the one with the lowest wave power density, while the lowest RCW values are observed at the most energetic site in North-West Sardinia. This behaviour can be explained by the fact that the dominant energetic waves in Sardinia are characterised by longer periods, due to the larger available fetch associated with prevailing north-westerly (Mistral) winds, with wave energy mainly concentrated in the 7–8 s range. In this period range, the system exhibits lower efficiency, as also highlighted by the RCW trends shown in Fig. 13.

5. Conclusions

This work presents a techno-economic analysis of a U-shaped sloshing tank Wave Energy Converter (U-WEC), assessing its performance

Table 6
Most occurrent sea state parameters and power density for the Mediterranean sites under analysis.

Parameter	Unit	CDS	GRGN	PNZ	SRD	PGL	UST
Most occurrent energetic period - T_e^*	(s)	4.60	4.95	4.50	4.50	4.10	4.10
Most occurrent significant wave height - H_s^*	(m)	0.50	0.30	0.35	0.30	0.50	0.30
Wave power density - P_w	(kW/m)	7.40	4.70	3.50	9.75	3.10	4.45
Latitude	(°N)	37.895	43.413	40.862	40.485	39.840	38.774
Longitude	(°E)	11.333	9.864	12.948	7.840	18.560	13.153

Table 7
Gross and net energy performance and efficiency of the optimal Wells turbines at the analysed Mediterranean sites.

Site	Site name	P_w (kW/m)	AEP_{gross} (MWh/y)		AEP_{net} (MWh/y)		RCW_{net} (%)	
			S	L	S	L	S	L
CDS	Strait of Sicily	7.40	142.3	257.0	113.4	187	7.1	11.6
UST	Ustica	4.45	90.9	155.1	72.3	113.3	7.6	11.7
SRD	North-West Sardinia	9.75	116.2	238.5	93.0	174.3	4.4	8.2
PGL	North-East Apulia	3.10	86.0	121.8	68.3	89.0	10.3	13.2
PNZ	Ponza	3.50	87.0	134.1	69.0	98.0	9.2	12.3
GRGN	Gorgona	4.70	91.1	158.6	72.1	115.7	7.0	11.3

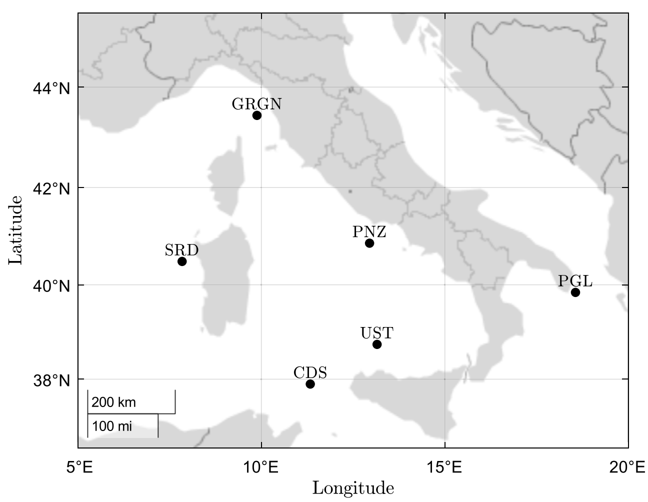

Fig. 14. Map of the analysed Mediterranean points.

at several Italian offshore sites of strategic interest, including locations suitable for co-location with offshore wind farms and off-grid islands. The system was optimised for a Mediterranean site in the Strait of Sicily and subsequently evaluated at additional locations, confirming its suitability for typical Mediterranean wave climates.

A two-stage optimisation framework was adopted. First, a techno-economic optimisation was performed on the main parameters governing displacement mass, used as a proxy for capital cost, and annual energy production. Second, an ad hoc optimisation of the Wells turbine was carried out for each device, accounting for the strong coupling between hull size, resonance behaviour, and turbine operating conditions. A comparison with a Northern European site highlighted the influence of different metocean conditions on the optimal system characteristics.

All optimisation outcomes consistently converged towards asymmetric hull configurations, indicating that the system benefits from enhanced hydrodynamic coupling among multiple degrees of freedom. This multi-DoF interaction, combined with resonance tuning between the hull and the U-tank, emerged as a key mechanism for maximising energy capture. The RCW proved to be an effective indicator for assessing site-device compatibility, showing that higher efficiency is achieved when dominant wave periods align with the system resonance. This also implies that optimal configurations are wave-climate-dependent, as confirmed by the comparison with the North Atlantic site, where longer dominant periods drive systematically different hull geometries and U-tank tuning.

It should be remarked that the present techno-economic assessment adopts displacement mass as a first-order proxy for cost. While this choice is consistent with the early-stage nature of the concept, it does not explicitly include other relevant contributions such as mooring, O&M, installation, and balance-of-plant costs, which may affect the final ranking of the optimal solutions.

Overall, the results demonstrate the applicability of the proposed U-WEC for Mediterranean offshore deployments, both in hybrid offshore wind applications and as a standalone solution for off-grid islands. Future work will focus on high-fidelity CFD modelling of the coupled U-tank and Wells turbine, and the development of real-time control strategies. Furthermore, in the future, an experimental campaign focused on selected Pareto-optimal configurations would strengthen the potential of the current preliminary model.

Finally, in future developments, the present methodology will be extended towards a fully integrated online co-design formulation, where hull geometry, U-tank tuning and Wells turbine sizing are optimised simultaneously in order to account more rigorously for mutual coupling effects across the full conversion chain. Future works will also include higher-fidelity nonlinear investigations under severe sea states, in order to assess survivability-related loads and quantify the impact of nonlinear hydrodynamic, sloshing, and pneumatic effects beyond the preliminary operational framework adopted herein. In order to quantify the impact of directional wave spreading, further analysis will investigate the assessment of multidirectional sea states incidence on device performance, resonance tuning, and optimal hull-U-tank robustness.

In conclusion, another natural extension of the present Mediterranean-focused analysis is to move towards a broader multi-site optimisation framework, with the aim of identifying recurrent wave-climate clusters and, in turn, grouping deployment sites and U-WEC design families according to their mutual similarity, transferability, and techno-economic affinity.

CRediT authorship contribution statement

Sergej Antonello Sirigu: Writing – review & editing, Writing – original draft, Visualization, Supervision, Software, Methodology, Investigation, Formal analysis, Data curation, Conceptualization. **Valerio Francesco Barnabei:** Writing – review & editing, Writing – original draft, Software, Methodology, Investigation, Data curation, Conceptualization. **Filippo Giorcelli:** Writing – review & editing, Writing – original draft, Visualization, Software, Methodology, Investigation, Formal analysis, Data curation. **Giovanni Delibra:** Supervision, Software, Methodology, Investigation, Formal analysis, Data curation, Conceptualization. **Alessandro Corsini:** Supervision, Resources, Project administration, Formal analysis, Conceptualization.

Declaration of competing interest

The authors declare the following financial interests/personal relationships which may be considered as potential competing interests: Filippo Giorcelli reports was provided by Ministry of University and Research. Valerio Barnabei reports financial support was provided by Ministry of University and Research. If there are other authors, they declare that they have no known competing financial interests or personal relationships that could have appeared to influence the work reported in this paper.

Acknowledgements

A preliminary version of the present article was presented at the 20th Sustainable Development of Energy, Water and Environment Systems Conference (SDEWES), which was held from 5–10 October 2025 in Dubrovnik, Croatia. The authors express their gratitude for the funds received from the Ministry of University and Research and PNRR's PhD scholarship program defined in DM-352/2022 in collaboration with Eni S.p.A. This publication is part of the PNRR-NGEU project. Moreover, the project is funded under the National Recovery and Resilience Plan (NRRP), Italy, Mission 4 Component 2 Investment 1.3 - Call for tender No. 1561 of 11.10.2022 of Ministero dell'Università e della Ricerca (MUR); funded by the European Union - NextGenerationEU Award Number: Project code PE0000021, Concession Decree No. 1561 of 11.10.2022 adopted by Ministero dell'Universita e della Ricerca (MUR), Italy, CUP, Italy E13C22001890001, Project title "Network 4 Energy Sustainable Transition - NEST.

References

[1] K. Gunn, C. Stock-Williams, Quantifying the global wave power resource, Renew. Energy 44 (2012) 296–304.
[2] S. Jin, S. Zheng, D. Greaves, On the scalability of wave energy converters, Ocean Eng. 243 (2022) 110212.
[3] A. Garcia-Teruel, D. Forehand, A review of geometry optimisation of wave energy converters, Renew. Sustain. Energy Rev. 139 (2021) 110593.
[4] L. Rusu, An evaluation of the synergy between the wave and wind energy along the west iberian nearshore, Energy Convers. Manag.: X 20 (2023) 100453.
[5] L. Wan, T. Moan, Z. Gao, W. Shi, A review on the technical development of combined wind and wave energy conversion systems, Energy 294 (2024) 130885.
[6] D. Curto, V. Franzitta, M. Trapanese, M. Cirrincione, A preliminary energy assessment to improve the energy sustainability in the small islands of the mediterranean sea, J. Sustain. Dev. Energy, Water Environ. Syst. 8 (4) (2020) 735–753.
[7] L. Liberti, A. Carillo, G. Sannino, Wave energy resource assessment in the mediterranean, the Italian perspective, Renew. Energy 50 (2013) 938–949, http://dx.doi.org/10.1016/j.renene.2012.08.023.
[8] D. Vicinanza, P. Contestabile, V. Ferrante, Wave energy potential in the north-west of sardinia (Italy), Renew. Energy 50 (2013) 506–521, http://dx.doi.org/10.1016/j.renene.2012.07.015.
[9] L. Rusu, An analysis of the environmental matrix in the adriatic sea–past and future projections, J. Sustain. Dev. Energy Water Environ. Syst. 12 (2) (2024) 1–21.
[10] J. Wu, W. Jiang, T. Yang, A bibliometric analysis of oscillating-water-column wave energy converters: emerging trends and research frontiers, Energy 340 (2025) 139365, http://dx.doi.org/10.1016/j.energy.2025.139365, URL https://www.sciencedirect.com/science/article/pii/S0360544225050078.
[11] M. Rosati, J. Henriques, J. Ringwood, Oscillating-water-column wave energy converters: A critical review of numerical modelling and control, Energy Convers. Manag.: X 16 (2022) 100322.
[12] T. Heath, Chapter 334 - the development and installation of the limpet wave energy converter, in: A. Sayigh (Ed.), World Renewable Energy Congress VI, Pergamon, Oxford, 2000, pp. 1619–1622, http://dx.doi.org/10.1016/B978-008043865-8/50334-2, URL https://www.sciencedirect.com/science/article/pii/B9780080438658503342.
[13] A.F. Falcão, A.J. Sarmento, L.M. Gato, A. Brito-Melo, The pico OWC wave power plant: Its lifetime from conception to closure 1986–2018, Appl. Ocean Res. 98 (2020) 102104, http://dx.doi.org/10.1016/j.apor.2020.102104, URL https://www.sciencedirect.com/science/article/pii/S0141118719305875.
[14] J. Lopez-Mendia, A. Aristondo, P. Ricci, J. Lekube, S. Ceballos, E. Robles, Improving the power production of mutriku wave power plant throughout tuning the actual generator and damping valve limits, Ocean Eng. 315 (2025) 119917, http://dx.doi.org/10.1016/j.oceaneng.2024.119917, URL https://www.sciencedirect.com/science/article/pii/S0029801824032554.
[15] C.L. Oikonomou, R.P. Gomes, L.M. Gato, Unveiling the potential of using a spar-buoy oscillating-water-column wave energy converter for low-power stand-alone applications, Appl. Energy 292 (2021) 116835.
[16] J. Portillo, P. Reis, J. Henriques, L. Gato, A. Falcão, Backward bent-duct buoy or frontward bent-duct buoy? Review, assessment and optimisation, Renew. Sustain. Energy Rev. 112 (2019) 353–368, http://dx.doi.org/10.1016/j.rser.2019.05.026, URL https://www.sciencedirect.com/science/article/pii/S1364032119303387.
[17] S.R. e Silva, R. Gomes, A. Falcao, Hydrodynamic optimization of the UGEN: Wave energy converter with U-shaped interior oscillating water column, Int. J. Mar. Energy 15 (2016) 112–126.
[18] L. Ciappi, L. Cheli, I. Simonetti, A. Bianchini, L. Talluri, L. Cappietti, G. Manfrida, Wave-to-wire models of wells and impulse turbines for oscillating water column wave energy converters operating in the mediterranean sea, Energy 238 (2022) 121585.
[19] F. Licheri, T. Ghisu, F. Cambuli, P. Puddu, Experimental characterization of a variable-pitch wells turbine, in: Journal of Physics: Conference Series, vol. 2893, (1) IOP Publishing, 2024, 012131.
[20] A. Castorrini, V.F. Barnabei, A. Corsini, F. Rispoli, K. Takizawa, T.E. Tezduyar, Computational fluid–structure interaction analysis of passive adaptive blades in turbomachinery applications, in: Frontiers in Computational Fluid-Structure Interaction and Flow Simulation: Research from Lead Investigators under Forty-2023, Springer, 2023, pp. 33–58.
[21] V.F. Barnabei, A. Castorrini, A. Corsini, F. Rispoli, FSI analysis and simulation of flexible blades in a wells turbine for wave energy conversion, in: E3S Web of Conferences, vol. 197, EDP Sciences, 2020, p. 11008.
[22] F. Giorcelli, P. Cabrera, B. Paduano, S.A. Sirigu, G. Mattiazzo, Energy system co-design approach for WECs optimisation: the pendulum wave energy converter case study, Appl. Energy 402 (2025) 126846.
[23] G. Vissio, D. Valério, G. Bracco, P. Beirão, N. Pozzi, G. Mattiazzo, ISWEC linear quadratic regulator oscillating control, Renew. Energy 103 (2017) 372–382.
[24] G. Malara, A. Romolo, V. Fiamma, F. Arena, On the modelling of water column oscillations in U-OWC energy harvesters, Renew. Energy 101 (2017) 964–972, http://dx.doi.org/10.1016/j.renene.2016.09.051.
[25] G. Palma, P. Contestabile, B. Zanuttigh, S.M. Formentin, D. Vicinanza, Integrated assessment of the hydraulic and structural performance of the OBREC device in the gulf of naples, Italy, Appl. Ocean Res. 101 (2020) 102217, http://dx.doi.org/10.1016/j.apor.2020.102217.
[26] A. Garcia-Teruel, O. Roberts, D.R. Noble, J.C. Henderson, H. Jeffrey, Design limits for wave energy converters based on the relationship of power and volume obtained through multi-objective optimisation, Renew. Energy 200 (2022) 492–504, http://dx.doi.org/10.1016/j.renene.2022.09.053.
[27] B. Guo, J.V. Ringwood, Geometric optimisation of wave energy conversion devices: A survey, Appl. Energy 297 (2021) 117100.
[28] F. Carapellese, B. Paduano, E. Pasta, G. Papini, N. Faedo, G. Mattiazzo, Nonlinear dynamic analysis and control synthesis for the swinging omnidirectional (SWINGO) wave energy converter, IFAC-PapersOnLine 56 (2) (2023) 11723–11728.
[29] K. Hasselmann, T.P. Barnett, E. Bouws, H. Carlson, D.E. Cartwright, K. Enke, J. Ewing, A. Gienapp, D. Hasselmann, P. Kruseman, et al., Measurements of wind-wave growth and swell decay during the joint north sea wave project (JONSWAP)., Ergaenzungsheft Zur Dtsch. Hydrogr. Z. Reihe A (1973).
[30] M. Bonfanti, N. Faedo, G. Mattiazzo, Towards efficient control synthesis for nonlinear wave energy conversion systems: impedance-matching meets the spectral-domain, Nonlinear Dynam. 112 (13) (2024) 11085–11109.
[31] O. Faltinsen, Sea loads on ships and offshore structures, vol. 1, Cambridge University Press, 1993.
[32] M. Folley, Numerical modelling of wave energy converters: state-of-the-art techniques for single devices and arrays, Academic Press, 2016.
[33] R. Kurnia, G. Ducrozet, NEMOH: Open-source boundary element solver for computation of first-and second-order hydrodynamic loads in the frequency domain, Comput. Phys. Comm. 292 (2023) 108885.
[34] A.R. Lloyd, Seakeeping: ship behaviour in rough weather, 1989.
[35] M. Fontana, G. Giorgi, M. Accardi, E. Giorcelli, S. Brizzolara, S.A. Sirigu, Numerical and experimental investigation of the dynamics of a u-shaped sloshing tank to increase the performance of wave energy converters, J. Mar. Sci. Eng. 11 (12) (2023) 2339.
[36] H.B. Bingham, Y.-H. Yu, K. Nielsen, T.T. Tran, K.-H. Kim, S. Park, K. Hong, H.A. Said, T. Kelly, J.V. Ringwood, R.W. Read, E. Ransley, S. Brown, D. Greaves, Ocean energy systems wave energy modeling task 10.4: Numerical modeling of a fixed oscillating water column, Energies 14 (6) (2021).

[37] J.J. Wijker, Random vibrations in spacecraft structures design: theory and applications, vol. 165, Springer Science & Business Media, 2009.
[38] N. Pozzi, Numerical modeling and experimental testing of a pendulum wave energy converter (PeWEC), 2018.
[39] S. Raghunathan, The wells air turbine for wave energy conversion, Prog. Aerosp. Sci. 31 (4) (1995) 335–386.
[40] A.F. Falcão, J.C. Henriques, Oscillating-water-column wave energy converters and air turbines: A review, Renew. Energy 85 (2016) 1391–1424.
[41] D. Bruschi, J. Fernandes, A. Falcão, C. Bergmann, Analysis of the degradation in the wells turbine blades of the pico oscillating-water-column wave energy plant, Renew. Sustain. Energy Rev. 115 (2019) 109368, http://dx.doi.org/10.1016/j.rser.2019.109368, URL https://www.sciencedirect.com/science/article/pii/S1364032119305763.
[42] Renexia Group, MED Wind project. URL https://medwind.it/.
[43] J. Orszaghova, S. Lemoine, H. Santo, P.H. Taylor, A. Kurniawan, N. McGrath, W. Zhao, M.V. Cuttler, Variability of wave power production of the M4 machine at two energetic open ocean locations: Off albany, western Australia and at EMEC, orkney, UK, Renew. Energy 197 (2022) 417–431.
[44] G. Korres, C. Oikonomou, D. Denaxa, M. Sotiropoulou, Mediterranean sea waves analysis and forecast (copernicus marine service MED-waves, MEDWAM4 system) (version 1) [data set], 2023, URL https://doi.org/10.25423/CMCC/MEDSEA_ANALYSISFORECAST_WAV_006_017_MEDWAM4.
[45] K. Deb, A. Pratap, S. Agarwal, T. Meyarivan, A fast and elitist multiobjective genetic algorithm: NSGA-II, IEEE Trans. Evol. Comput. 6 (2) (2002) 182–197.
[46] A. Shadmani, M.R. Nikoo, A.H. Gandomi, M. Chen, R. Nazari, Advancements in optimizing wave energy converter geometry utilizing metaheuristic algorithms, Renew. Sustain. Energy Rev. 197 (2024) 114398.
[47] S.H. Salter, et al., Wave power, Nature 249 (5459) (1974) 720–724.
[48] 4C Offshore Ltd., Global offshore wind farm map, 2025, https://map.4coffshore.com/offshorewind/. (Accessed: 18 December 2025).